Heat release effects on the Reynolds stress budgets in turbulent premixed jet flames at low and high Karlovitz numbers

Jinyoung Lee^{a,*}, Jonathan F. MacArt^b, Michael E. Mueller^a

^aDepartment of Mechanical and Aerospace Engineering, Princeton University, Princeton, NJ 08544, USA ^bDepartment of Aerospace and Mechanical Engineering, University of Notre Dame, Notre Dame, IN 46556, USA

Abstract

In turbulent premixed flames at low Karlovitz number, combustion heat release can have a significant impact on turbulence. Thermal expansion in flame induces dilatation, and the corresponding pressure-dilatation correlation acts as a primary source of turbulent kinetic energy (TKE). As a consequence, the flame-normal component of the normal Reynolds stresses significantly increases. Additionally, for sheared flames, typical of jet flames, the shear component of the Reynolds stresses exhibits counter-Boussinesq behavior. For flames at low Karlovitz number, where these effects dominate, no models have successfully predicted all Reynolds stress components. To develop more complete turbulence models, heat release effects on the evolution of all Reynolds stress components need to be analyzed. In this work, Reynolds stress budgets are evaluated from Direct Numerical Simulation (DNS) databases of spatially-evolving turbulent premixed planar jet flames at low and high Karlovitz numbers. In the Reynolds stress budgets, the velocitypressure gradient correlation term is important at both Karlovitz numbers but serves fundamentally different roles in each case. In the budgets for the normal components, the velocity-pressure gradient correlation term is decomposed into a redistribution term and an isotropic term, where the redistribution term acts to redistribute energy between the Reynolds stress components and the isotropic term is the pressure-dilatation source term of turbulent kinetic energy. At high Karlovitz number, the isotropic term is negligible, and the redistribution term acts to isotropize the turbulence as in non-reacting flows. Conversely, at low Karlovitz number, the isotropic term acts as a large source, and the redistribution term preferentially injects energy into the flame-normal component at the expense of other components which acts to make the turbulence less isotropic. In the budget for the shear component, the shear production term dominates the velocity-pressure gradient correlation term at high Karlovitz number, but the opposite is observed at low Karlovitz number. The dominance of the velocity-pressure gradient correlation term at low Karlovitz number is primarily induced by the flame-generated mean pressure gradient and ultimately leads to the counter-Boussinesq behavior of the shear component. The overall analysis indicates that any turbulence model that relies on small-scale isotropy and/or rapid isotropization will fail to capture the heat release effects on turbulence at low Karlovitz number. Keywords: Turbulent premixed combustion, Reynolds stress budget, Direct Numerical Simulation

Email address: j150@princeton.edu (Jinyoung Lee)

^{*}Corresponding author

1. Introduction

Turbulent combustion is characterized by nonlinear interactions between turbulence and combustion heat release. The heat release induces thermal expansion, that is, flow dilatation, and accelerates the flow velocity in the flamenormal direction. Bilger [1] has argued that, when the time scales of this combustion-induced dilatation are faster than those of the turbulence-induced strain, heat release should have a significant influence on the turbulence structure; Hamlington et al. [2] have made a similar argument that turbulence is weakly affected by combustion heat release at high turbulence intensity. Based on these arguments, for the purpose of the scaling of heat release effects on the turbulence, MacArt et al. [3] defined a critical Karlovitz number as $Ka_{cr} \equiv \rho_u/\rho_b - 1$, where ρ_u is the density of the unburned gas, and ρ_b is the density of the burned gas. The local Karlovitz number is defined as $Ka \equiv \tau_F/\tau_\eta$, where $\tau_{\rm F}$ is the flame time scale, and τ_{η} is the Kolmogorov time scale. When the local Karlovitz number is less than the critical Karlovitz number, that is, Ka « Ka_{cr}, the heat release effects on the turbulence are expected to be dominant and vice versa. MacArt et al. [3] confirmed this scaling in a parametric Direct Numerical Simulation (DNS) study of low Mach number spatially-evolving turbulent premixed planar jet flames at low and high Karlovitz numbers. In the turbulent kinetic energy (TKE) budget, at high Karlovitz number, production by mean shear is the dominant source of the TKE and is balanced by viscous dissipation, and pressure-dilatation is negligible. However, at low Karlovitz number, pressure-dilatation is the dominant source of the TKE and is balanced by both viscous dissipation and production by mean shear, which become sinks of TKE. In addition, while the scalar flux and the Reynolds stresses are conventionally modeled using the gradient-transport and the Boussinesq hypothesis, respectively, at low Karlovitz number, the scalar flux actually exhibits counter-gradient behavior, and the Reynolds stresses exhibit analogous "counter-Boussinesq" behavior. Conventional models work only at high Karlovitz number where the influence of heat release is diminished. Therefore, when heat release strongly affects turbulence, the use of conventional turbulence models originally developed for non-reacting flows is fundamentally flawed.

Several efforts have been undertaken to develop turbulence models accounting for heat release effects on turbu-lence. For premixed flames in the zero Karlovitz number limit, that is, an infinitely thin flame, the Bray-Moss-Libby (BML) framework has been used to model the scalar flux and the Reynolds stresses [4]. In addition, in order to model the scalar flux for premixed flames at finite Karlovitz number, Veynante et al. [5] linearly combined the BML model and the gradient-transport model, which is valid in the infinite Karlovitz number limit. For premixed flames in isotropic turbulence, this scalar flux model was able to capture the transition of the flame-normal scalar flux from counter-gradient transport to gradient transport. Their work was extended to also model the Reynolds stresses for premixed flames at finite Karlovitz number by MacArt et al. [3] by combining the BML model and the conventional model based on the Boussinesq hypothesis. This Reynolds stress model was able to capture the significant increase in the flame-normal component of the normal Reynolds stresses resulting from the heat release effects. However, the flame-parallel normal components and the counter-Boussinesq behavior of the shear component of the Reynolds stresses were not accurately predicted. MacArt et al. [3] speculated that the Reynolds stress models based on the com-

bination of the BML framework and the Boussinesq hypothesis miss the effects of pressure redistribution of energy between the Reynolds stress components. This hypothesis needs to be evaluated to develop a more accurate Reynolds stress model.

The aim of this work is to fully characterize the heat release effects on the evolution of all Reynolds stress components, not just the turbulent kinetic energy [3], by evaluating and comparing the Reynolds stress budgets from turbulent premixed planar jet flames at low and high Karlovitz numbers, which are below and above the critical Karlovitz number, respectively. From the budget analysis, the influences of pressure redistribution are specifically investigated, and a more complete understanding of counter-Boussinesq behavior of the shear component is developed. Previous studies that have analyzed the heat release effects on the Reynolds stress budgets relied on configurations of premixed statistically planar flames in isotropic turbulence without large-scale shear and corresponding non-zero shear component of the Reynolds stresses, limiting their analyses to the flame-normal component [6, 7, 8].

An outline of the paper is as follows. In Section 2, the DNS databases are described in detail. In Section 3, the turbulence statistics including the Reynolds stress components and the Reynolds stress budgets are evaluated and compared between two Karlovitz number cases. The pressure redistribution processes in the Reynolds stress budgets are analyzed in detail regarding their role in the evolution of the Reynolds stresses. In Section 4, based on these insights, the inter-dependence between the effects of large-scale shear and the flame on the shear component of the Reynolds stresses are further discussed. In Section 5, results and implications for turbulence modeling are summarized.

2. Direct Numerical Simulations

Previous DNS databases [3] of spatially-evolving turbulent premixed planar jet flames at low and high Karlovitz numbers have been analyzed in this work. The DNS configuration consists of a turbulent central jet of a stoichiometric hydrogen-air mixture diluted with nitrogen (20% by volume to prevent flashback) and laminar coflow jets of equilibrium products. For this mixture, a reaction progress variable is defined as the normalized oxygen mass fraction:

$$C = \frac{Y_{O_2,u} - Y_{O_2}}{Y_{O_2,u} - Y_{O_2,b}},\tag{1}$$

where $Y_{\text{O}_2,\text{u}}$ and $Y_{\text{O}_2,\text{b}}$ are the oxygen mass fraction in the unburned and burned gas mixtures, respectively. The bulk Reynolds number defined as $\text{Re}_0 \equiv U_0 H_0/\nu$, where U_0 and H_0 are the velocity and height of the central jet, respectively, and ν is the kinematic viscosity, is $\text{Re}_0 = 5,000$ for both Karlovitz number cases. For this fuel-air mixture, the laminar flame speed is $s_L = 1.195$ m/s, the laminar flame thickness is $\delta_F = 0.435$ mm, and the critical Karlovitz number is $Ka_{\text{cr}} = 6.7$. The in-flame Karlovitz number $Ka_{\tilde{C}=0.5}$, defined where the density-weighted mean progress variable is 0.5, is greater than Ka_{cr} at high Karlovitz number (Case K2) and less than Ka_{cr} at low Karlovitz number (Case K1). The in-flame Damköhler number $Da_{\tilde{C}=0.5}$, where $Da \equiv \tau_1/\tau_F$ and τ_1 is the integral time scale, is

 $_{66}$ 0.05 for Case K2 and 0.60 for Case K1. The domain sizes in the streamwise, cross-stream, and spanwise directions are $24H_0 \times 16H_0 \times 3H_0$ for Case K2 and $12H_0 \times 24H_0 \times 3H_0$ for Case K1. Simulation parameters at the streamwise location $x/H_0 = 3$ are summarized in Table 1.

[Table 1 about here.]

The transport equations for mass, momentum, species mass fractions, and temperature with the ideal gas equation of state are solved using a low Mach number, semi-implicit, iterative, finite difference solver with a structured grid in Cartesian coordinates [9, 10]. For chemistry, a detailed nine species hydrogen chemical kinetic model is used [11]. For molecular transport, a constant non-unity Lewis number, which has been validated for laminar and turbulent premixed hydrogen-air flames by Burali *et al.* [12], is used for each species.

The streamwise, cross-stream, and spanwise directions are denoted by x, y and z, respectively. The spanwise direction z is statistically homogeneous. Statistics are averaged in the spanwise direction z and time t over approximately 29.7 (Case K2) and 47.9 (Case K1) centerline integral times and collected at the streamwise location $x/H_0 = 3$ for both Karlovitz number cases. Convergence of the statistics have been confirmed by also considering half as much data. In addition, the results at downstream locations have been examined and provide qualitatively similar conclusions drawn at the upstream location $x/H_0 = 3$ regarding the underlying physics.

For a quantity ϕ , means and fluctuations are denoted by $\bar{\phi}$ and $\phi' \equiv \phi - \bar{\phi}$, respectively, and density-weighted means and fluctuations are denoted by $\tilde{\phi} \equiv \overline{\rho\phi}/\bar{\rho}$ and $\phi'' \equiv \phi - \tilde{\phi}$, respectively. Because all of the statistics analyzed in this work are (anti-)symmetric about the jet centerline, figures below show the statistics only for one side of the centerline in the positive y-direction. To facilitate comparison of the two Karlovitz number cases, all statistics are plotted against the density-weighted mean progress variable \tilde{C} rather than the corresponding cross-stream physical coordinate y. In addition, the local centerline streamwise velocity \tilde{U}_{cl} , the local centerline density $\bar{\rho}_{cl}$, and the jet halfwidth $y_{1/2}$ are used for normalizing the results. In order to reduce the influence of numerical error on the higher-order statistics considered in this work, the DNS databases have been recomputed, compared to MacArt *et al.* [3], with a larger number of sub-iterations used to converge the implicit mid-point method for time advancement, resulting in negligibly small residuals in each of the budgets shown in subsequent figures.

Additional details about the DNS databases can be found in Ref. [3].

3. Results

3.1. Reynolds Stress Budgets

The components of the density-weighted Reynolds stresses $R_{ij} \equiv \widetilde{u_i u_j} - \widetilde{u}_i \widetilde{u}_j$, normalized by $\widetilde{U}_{\rm cl}^2$, are shown in Figure 1, which is also shown in Ref. [3] but is reproduced here from the recomputed DNS databases to facilitate discussion of the Reynolds stress budgets; the non-density-weighted Reynolds stresses are qualitatively similar and are included in Appendix A. For Case K2, due to the minimal influence of combustion heat release, the overall profiles

 of the Reynolds stress are similar to non-reacting turbulent shear flows [13]. The largest component is the streamwise component R_{11} because the streamwise velocity is fastest; the cross-stream component R_{22} and the spanwise component R_{33} are much smaller than R_{11} . In addition, the shear component R_{12} is positive for all \tilde{C} , while the gradient of the streamwise velocity in the cross-stream direction $(\partial \tilde{u}_1/\partial x_2)$ is negative. This is qualitatively consistent with the Boussinesq hypothesis. For Case K1, R_{22} increases significantly through the flame because the flow velocity accelerates in the flame-normal direction due to thermal expansion and the flame-normal vector is mostly aligned with the cross-stream direction [3]. In addition, it is important to note that the sign of R_{12} is negative for $\tilde{C} > 0.1$, even though $\partial \tilde{u}_1/\partial x_2$ is negative for all \tilde{C} . This is inconsistent with the Boussinesq hypothesis and results from the influence of heat release; in other words, the Reynolds stresses are not anti-aligned with the strain rate tensor. This mechanism will be investigated in the remainder of this paper through the analysis of the Reynolds stress budgets.

[Figure 1 about here.]

The Reynolds stress transport equations describe the evolution of the R_{ij} components:

$$\underbrace{\frac{\partial \bar{\rho}R_{ij}}{\partial t}}_{B0} = \underbrace{-\frac{\partial}{\partial x_k} \left(\bar{\rho}\tilde{u}_k R_{ij} \right)}_{B1} \underbrace{-\frac{\partial}{\partial x_k} \left(\bar{\rho}u_k''u_i''u_j'' \right)}_{B2} \underbrace{+\frac{\partial}{\partial x_k} \left(\overline{\tau_{jk}u_i''} \right) + \frac{\partial}{\partial x_k} \left(\overline{\tau_{ik}u_j''} \right)}_{B3} \underbrace{-\frac{\partial}{\partial x_k} \left(\overline{\tau_{ik}u_i''} \right) + \frac{\partial}{\partial x_k} \left(\overline{\tau_{ik}u_i''} \right) + \frac{\partial}{\partial x_k} \left(\overline{\tau_{ik}u_j''} \right)}_{B3} \underbrace{-\frac{\partial}{\partial x_k} \left(\overline{\tau_{ik}u_i''} \right) + \frac{\partial}{\partial x_k} \left(\overline{\tau_{ik}u_i''} \right) + \frac{\partial}{\partial x_k} \left(\overline{\tau_{ik}u_j''} \right)}_{B3} \underbrace{-\frac{\partial}{\partial x_k} \left(\overline{\tau_{ik}u_i''} \right) + \frac{\partial}{\partial x_k} \left(\overline{\tau_{ik}u_i''} \right) + \frac{\partial}{\partial x_k} \left(\overline{\tau_{ik}u_j''} \right)}_{B3} \underbrace{-\frac{\partial}{\partial x_k} \left(\overline{\tau_{ik}u_i''} \right) + \frac{\partial}{\partial x_k} \left(\overline{\tau_{ik}u_i''} \right) + \frac{\partial}{\partial x_k} \left(\overline{\tau_{ik}u_j''} \right)}_{B3} \underbrace{-\frac{\partial}{\partial x_k} \left(\overline{\tau_{ik}u_i''} \right) + \frac{\partial}{\partial x_k} \left(\overline{\tau_{ik}u_i''} \right) + \frac{\partial}{\partial x_k} \left(\overline{\tau_{ik}u_j''} \right)}_{B3} \underbrace{-\frac{\partial}{\partial x_k} \left(\overline{\tau_{ik}u_i''} \right) + \frac{\partial}{\partial x_k} \left(\overline{\tau_{$$

The terms in Eq. 2 correspond to the following: unsteadiness (B0), convective transport (B1), turbulent transport (B2), viscous transport (B3), velocity-pressure gradient correlation (B4), shear production (B5), and viscous dissipation (B6). Figure 2 shows the Reynolds stress budgets, normalized by $\bar{\rho}_{cl}\tilde{U}_{cl}^3/y_{1/2}$, for both Cases K2 and K1. For Case K2, although the velocity-pressure gradient correlation term is negligible in the TKE budget [3], it is important in the budgets for the normal components of the Reynolds stresses, extracting energy (negative) from the largest component (R_{11}) and injecting energy (positive) into the smaller components (R_{22}) and (R_{33}) . Therefore, the velocity-pressure gradient correlation term acts to isotropize the turbulence as in non-reacting flows [14]. In the budget for R_{12} , the negative velocity-pressure gradient correlation term is consistent with a return to isotropy since R_{12} is positive, and R_{12} remains positive due to the influence of the large positive shear production term. For Case K1, the velocitypressure gradient correlation term is also the dominant source in the budget for R_{22} in most of the flame (Figure 2d). However, unlike Case K2, in Case K1, R_{22} is the largest normal component of the Reynolds stresses, so the velocitypressure gradient correlation term acts to make the turbulence less isotropic. The velocity-pressure gradient is also positive, albeit smaller in magnitude, for the other normal components of the Reynolds stresses. In the budget for R_{12} , the velocity-pressure gradient correlation term is negative and has the largest magnitude of all terms for $\tilde{C} < 0.4$, which results in a negative shear component of the Reynolds stresses. The velocity-pressure gradient correlation term having the same sign as the shear component of the Reynolds stresses is inconsistent with a return to isotropy.

3.2. Decomposition of Velocity-Pressure Gradient Correlation

Comparing the two Karlovitz number cases, the velocity-pressure gradient correlation plays a fundamentally different role. At high Karlovitz number, this term acts to isotropize the turbulence as in non-reacting flows, but, at low Karlovitz number, this term reinforces anisotropy. To investigate these differences, the velocity-pressure gradient correlation term can be decomposed into two terms in variable density flows, a redistribution term (Φ_{ij}) and an isotropic term (Π_{ij}) [15, 16]:

$$\underbrace{-u_{i}^{"}\frac{\partial p}{\partial x_{j}} - u_{j}^{"}\frac{\partial p}{\partial x_{i}}}_{\text{B4}} = \underbrace{\left(-u_{i}^{"}\frac{\partial p}{\partial x_{j}} - \overline{u_{j}^{"}\frac{\partial p}{\partial x_{i}}} + \frac{2}{3}\overline{u_{k}^{"}\frac{\partial p}{\partial x_{k}}}\delta_{ij}\right)}_{\Phi_{ii}} \underbrace{-\frac{2}{3}\overline{u_{k}^{"}\frac{\partial p}{\partial x_{k}}}\delta_{ij}}_{\Pi_{ij}}.$$
(3)

The isotropic term appears in the TKE budget and includes the pressure-dilatation source term as well as the pressure transport term. In the redistribution term, the trace of the velocity-pressure gradient correlation term is subtracted from itself. Therefore, the redistribution term does not appear in the TKE budget and has no direct contribution to the evolution of the TKE. Instead, the redistribution term works to redistribute energy between the R_{ij} components. For the normal components of R_{ij} , Figure 3 shows the decomposition of the velocity-pressure gradient correlation term in Eq. 3, normalized by $\bar{\rho}_{cl}\tilde{U}_{cl}^3/y_{1/2}$. For Case K2, the isotropic term is negligible as expected from the fact that the pressure-dilatation is negligible in the TKE budget. The streamwise component of the redistribution term (Φ_{11}) is negative, while other components of the redistribution term (Φ_{22}) and Φ_{33} are positive. The role of the velocity-pressure gradient correlation term for Case K2 becomes more clear, isotropizing the turbulence through the redistribution term by acting to move energy from the largest normal component to the smaller normal components. For Case K1, the isotropic term is large and positive as expected from the fact that the pressure-dilatation is the dominant source in the TKE budget. The cross-stream component of the redistribution term (Φ_{22}) is positive, while other components of the redistribution term (Φ_{11} and Φ_{33}) are negative. Therefore, the sign of the redistribution term is essentially opposite to Case K2, preferentially injecting energy into the largest flame-normal component (R_{22}) and increasing its relative magnitude at the expense of other components. This reinforcement of the anisotropy is driven by the thermal expansion in the flame, which is inherently anisotropic.

[Figure 3 about here.]

In the budget for R_{12} , the velocity-pressure gradient correlation term can be further decomposed into mean pressure terms $(\phi_{ij}^{(m)})$ and fluctuating pressure terms $(\phi_{ij}^{(f)})$ [16]:

$$\underbrace{-\overline{u_{1}''}\frac{\partial p}{\partial x_{2}} - \overline{u_{2}''}\frac{\partial p}{\partial x_{1}}}_{\text{B4} (=\Phi_{12})} = \underbrace{-\overline{u_{1}''}\frac{\partial \bar{p}}{\partial x_{2}}}_{\phi_{12}^{(m)}} \underbrace{-\overline{u_{1}''}\frac{\partial p'}{\partial x_{2}}}_{\phi_{12}^{(f)}} \underbrace{-\overline{u_{2}''}\frac{\partial \bar{p}}{\partial x_{1}}}_{\phi_{21}^{(m)}} \underbrace{-\overline{u_{2}''}\frac{\partial p'}{\partial x_{1}}}_{\phi_{21}^{(f)}}.$$
(4)

Figure 4 shows the decomposition of the velocity-pressure gradient correlation term in Eq. 4, normalized by $\bar{\rho}_{cl}\tilde{U}_{cl}^3/y_{1/2}$. For Case K2, the mean pressure terms are much smaller in magnitude than the fluctuating pressure terms. At high Karlovitz number, hydrodynamic effects dominate over flame effects, and the mean pressure gradient in a free jet is very small. Therefore, the return to isotropy, that is, the sink in the budget for the positive R_{12} , is due primarily to the influence of the fluctuating pressure gradient. Conversely, for Case K1, the mean pressure terms are larger in magnitude than the fluctuating pressure terms. Therefore, the mean pressure term $\phi_{12}^{(m)}$ is the dominant and negative source term in the budget for R_{12} and primarily causes the counter-Boussinesq behavior of R_{12} . $\phi_{12}^{(m)}$ has large and negative values for two reasons. First, the flame generates a negative mean pressure gradient in the flame-normal direction (that is, $-\partial \bar{p}/\partial x_2 > 0$) due to thermal expansion, which is dominant over hydrodynamic effects at low Karlovitz number. Second, $\overline{u_1''}$ is negative due to the correlation of the density and velocity fluctuations. The mean of the density-weighted fluctuations can be written as

$$\overline{u_1''} = -\frac{\overline{\rho' u_1'}}{\bar{\rho}}.\tag{5}$$

In the present DNS configuration, reactants have a faster streamwise velocity and are denser than the products. Therefore, the density fluctuations and streamwise velocity fluctuations are positively correlated, and $\overline{u_1''}$ is negative according to Eq. 5.

[Figure 4 about here.]

4. Discussion

The decomposition of the velocity-pressure gradient correlation term in the budget for R_{12} demonstrates the importance of the mean pressure term in the development of the counter-Boussinesq behavior of R_{12} in low Karlovitz number flames. This term depends on both the sign of the pressure gradient, which is negative from reactants to products, and the sign of $\overline{u_1''}$, which depends on the sign of the correlation of the density and streamwise velocity fluctuations so would depend on whether the streamwise velocity of the reactants is faster or slower compared to the products.

Figure 5 shows two different configurations of the flame and the reactants/products streams. The mean streamwise velocity of the reactants stream is faster than that of the products stream in the first configuration shown in Figure 5a and vice versa in the second configuration shown in Figure 5b. In other words, in the two configurations, only the sign of the shear $\partial \tilde{u}_1/\partial x_2$ is reversed: $\partial \tilde{u}_1/\partial x_2 < 0$ in the first and $\partial \tilde{u}_1/\partial x_2 > 0$ in the second. The first corresponds to the present DNS configuration. The correlation of the density and velocity fluctuations becomes opposite in sign for two configurations such that $\overline{u_1''}$ is negative in the first and is positive in the second. For both configurations, at low Karlovitz number, the mean pressure gradient in the flame-normal direction is negative, that is, $-\partial \bar{p}/\partial x_2 > 0$. Therefore, the dominant mean pressure term $\phi_{12}^{(m)}$ ($\equiv -\overline{u_1''} \partial \bar{p}/\partial x_2$) and the corresponding R_{12} become negative in

 the first configuration and become positive in the second configuration. However, since the sign of the shear is also reversed, in both cases, $\phi_{12}^{(m)}$ induces the counter-Boussinesq behavior of R_{12} .

[Figure 5 about here.]

Through this simple thought experiment with the alternative configuration, the interactions between the large-scale shear and the flame are important in determining the sign of the shear component of the Reynolds stresses but ultimately do not affect the inducement of the counter-Boussinesq behavior of shear component of the Reynolds stresses by the flame. In other words, there is no competition between the large-scale shear and the flame in determining whether the shear component of the Reynolds stresses is Boussinesq or counter-Boussinesq; the shear component of the Reynolds stresses is always counter-Boussinesq in low Karlovitz number flames. The interactions between the large-scale shear and the flame have been overlooked in most previous works that have considered statistically planar flame configurations without large-scale shear.

In addition to indirectly influencing the sign of the velocity pressure gradient correlation, the sign of the shear directly influences the sign of shear production. The shear production term in the budget for R_{12} can be simplified since the gradients in the streamwise and spanwise directions are smaller than the gradients in the cross-stream direction:

$$-\bar{\rho}R_{k1}\frac{\partial \tilde{u}_2}{\partial x_k} - \bar{\rho}R_{k2}\frac{\partial \tilde{u}_1}{\partial x_k} \approx -\bar{\rho}R_{12}\frac{\partial \tilde{u}_2}{\partial x_2} - \bar{\rho}R_{22}\frac{\partial \tilde{u}_1}{\partial x_2}.$$
 (6)

At low Karlovitz number, $\partial \tilde{u}_2/\partial x_2$ in the first term on the right hand side of Eq. 6 is large and positive for both configurations due to the velocity acceleration in the flame-normal direction. Therefore, the sign of the first term is always opposite to the sign of R_{12} . This means that for both configurations considered, the first term opposes the influence of the mean pressure term $\phi_{12}^{(m)}$ in the evolution of R_{12} . However, the magnitude of this first shear production term is less than the magnitude of the pressure gradient term for smaller values of the progress variable. At low Karlovitz number, the second term in Eq. 6 can be argued to scale with $\rho_c s_L^2 \Delta U/l$, where ρ_c is the characteristic gas density, $s_{\rm L}$ is the laminar flame speed, ΔU is the bulk streamwise velocity difference between the reactants and products streams, and l is the bulk flow length scale. However, $\phi_{12}^{(m)}$ can be argued to scale with $\rho_c s_L^2 \Delta U / \delta_F$, where δ_F is the laminar flame thickness. Because δ_F is much thinner than l at low Karlovitz number, the second term in Eq. 6 is much smaller in magnitude than $\phi_{12}^{(m)}$. Note that the scaling of the first term of the shear production term can be argued to scale similarly to the mean pressure term $\phi_{12}^{(m)}$, if the shear component of the Reynolds stresses is taken to scale as $s_L\Delta U$. Conversely, at high Karlovitz number, the second term in Eq. 6 is expected to scale as $\rho_c u'^2 \Delta U/l$, where u' is the turbulence intensity, and dominates over the first term in Eq. 6 and the velocity-pressure gradient correlation term. As a final note, at high Karlovitz number, the mean pressure gradient has been found to play a negligible role in the evolution of the Reynolds stresses (or other quantities such as the vorticity [17]). However, this conclusion is strongly influenced by the fact that the free jet considered here has no significant mean hydrodynamic pressure gradient. For flows with a large mean hydrodynamic pressure gradient, this pressure gradient has been shown to strongly interact with the flame through the baroclinic production of vorticity [18]. The influence of such externally imposed pressure gradients on the Reynolds stresses at high Karlovitz number is beyond the scope of the current work but is certainly worthy of future investigation.

5. Conclusions

 Reynolds stress budgets have been evaluated to analyze heat release effects on the Reynolds stresses in turbulent premixed jet flames at low and high Karlovitz numbers. The velocity-pressure gradient correlation term in the budgets serves fundamentally different roles at the two Karlovitz numbers. At high Karlovitz number, the velocity-pressure gradient correlation term acts to isotropize the turbulence as in non-reacting flows, while, at low Karlovitz number, the term becomes the dominant source of the largest flame-normal component and makes the turbulence less isotropic.

In the budgets for the normal components, the velocity-pressure gradient correlation term is decomposed into a redistribution term and an isotropic term. At high Karlovitz number, the isotropic term is negligible as expected from the fact that the pressure-dilatation is negligible in the TKE budget. The redistribution term extracts energy from the largest component and injects energy into smaller components. This corresponds to the classical return to isotropy. On the other hand, at low Karlovitz number, the isotropic term is large as expected from the fact that the pressure-dilatation is the dominant source in the TKE budget. The redistribution term preferentially injects energy into the flame-normal component at the expense of other components. This is associated with anisotropic dilatation effects in the flame.

In the budget for the shear component, the velocity-pressure gradient correlation term is decomposed into a mean pressure term and a fluctuating pressure term. At high Karlovitz number, since there is no mean hydrodynamic pressure gradient, the fluctuating pressure dominates. Conversely, at low Karlovitz number, the velocity-pressure gradient correlation term is dominated by the mean pressure gradient established by the flame. The large magnitude of this term leads to the counter-Boussinesq behavior of the shear component of the Reynolds stresses.

Based on the budget analyses, two challenges in turbulence modeling for turbulent premixed combustion at low Karlovitz number are explicitly highlighted. First, the conventional assumption of nearly isotropic turbulence, which is the basis of the Boussinesq hypothesis, is not valid when the anisotropic dilatation effects in the flame are dominant. Second, the indirect influence of the heat release through redistribution via the velocity-pressure gradient correlation term needs to be considered and cannot simply be assumed to isotropize the turbulence. More comprehensive models that resolve these challenges are required to adequately capture heat release effects on turbulence, and three possible approaches for modeling the Reynolds stresses in low Karlovitz number premixed flames are summarized here.

 One potential approach is to generalize the Boussinesq model to capture the redistribution between the Reynolds stress components. Speziale [19] has reviewed the development of nonlinear generalizations of the Boussinesq

model, which can relax the purely dissipative nature of the standard Boussinesq model and account for higherorder and nonlinear processes generating anisotropy in the Reynolds stresses. Because those models have been developed for non-reacting flow, modifications should be made by considering the heat release effects on the turbulence, especially for determining the nonlinear model parameters.

- Another approach is to simply solve the Reynolds stress transport equations. However, closure models for the unclosed terms in the Reynolds stress transport equations, which have been developed for non-reacting flows, are unlikely to be valid for the flames at low Karlovitz number. Specifically, the model for the velocity-pressure gradient correlation term must be able to capture the fundamentally different role of this term between low and high Karlovitz number regimes. Lipatnikov and Chomiak [8] have reviewed modeling efforts that consider heat release effects on the turbulence in the context of closing the Reynolds stress transport equations. However, most previous work is limited to flames without large-scale shear and do not consider the shear component of the Reynolds stresses. In this work, the dominant terms in the budget for the shear component have been analyzed and discussed in detail, and these insights could be leveraged in future studies for the development of closure models for the Reynolds stress transport equations.
- Finally, MacArt *et al.* [20] have recently proposed an integrated modeling approach to account for the heat release effects on the turbulence based on conditional averaging with respect to the flame structure variable. The rationale for this approach is that development of algebraic turbulence models or even closure for the Reynolds stress transport equations is extremely challenging in the low Karlovitz number regime since the models must capture both the effects of the flame dynamics (i.e., the effects of the local flame motion) and the direct effects of the heat release (i.e., all heat release effects except for the flame dynamics) on the turbulence. By utilizing the flame conditioning, the flame dynamics are removed, isolating the direct heat release effects. The major findings in this work, particularly with respect to the role of the pressure-related terms, could be helpful in developing closure models in this new turbulence modeling framework.

As a final note, for the high Karlovitz number case (Case K2), all scales of the turbulence are faster than the flame (Da < 1). For the low Karlovitz number case (Case K1), all scales of the turbulence are slower than the flame (Ka < Ka_{cr}). Therefore, the two Karlovitz number cases can be considered as the limiting cases. When the Karlovitz number is fixed, an increase in the Reynolds number is accompanied by an increase in the Damköhler number. By increasing the Damköhler number at the high Karlovitz number case, an intermediate regime, where $Ka > Ka_{cr}$ and Da > 1, could be realized. In this intermediate regime, the flame is slower and larger than the Kolmogorov scale of the turbulence but faster and smaller than the integral scale of the turbulence. However, the Reynolds numbers required to reach such a regime with significant scale separation between the Kolmogorov scale, the flame, and the integral scale are well beyond current computational capabilities (trillions of grid points scaling up the present simulations). However, such a regime is certainly worthy of future investigation.

Acknowledgements

The authors gratefully acknowledge funding from the National Science Foundation, Award CBET-1839425, and valuable support in the form of computational time on the TIGRESS high performance computing center at Princeton University, which is jointly supported by the Princeton Institute for Computational Science and Engineering (PICSciE) and the Princeton University Office of Information Technology's Research Computing department.

Appendix A. Non-Density-Weighted Reynolds Stress Components

Another common assumption in turbulence modeling for reacting flows is modeling the density-weighted Reynolds stresses using models for the non-density-weighted Reynolds stresses in non-reacting flows. The density-weighted Reynolds stresses are shown in Figure 6, where both are normalized by \tilde{U}_{cl}^2 . For Cases K2 and K1, the density-weighted and non-density-weighted Reynolds stresses are qualitatively similar with only slight differences in the peak locations and the magnitudes resulting from the weighting by density.

[Figure 6 about here.]

References

- [1] R. W. Bilger, Some aspects of scalar dissipation, Flow, Turbul. Combust. 72 (2004) 93–114.
- [2] P. E. Hamlington, A. Y. Poludnenko, E. S. Oran, Interactions between turbulence and flames in premixed reacting flows, Phys. Fluids 23 (2011) 125111.
- J. F. MacArt, T. Grenga, M. E. Mueller, Effects of combustion heat release on velocity and scalar statistics in turbulent premixed jet flames at
 low and high Karlovitz numbers, Combust. Flame 191 (2018) 468–485.
- [4] K. N. C. Bray, P. A. Libby, J. B. Moss, Unified modeling approach for premixed turbulent combustion-part I: General formulation, Combust. Flame 61 (1985) 87–102.
- [5] D. Veynante, A. Trouvé, K. N. C. Bray, T. Mantel, Gradient and counter-gradient scalar transport in turbulent premixed flames, J. Fluid
 Mech. 332 (1997) 263–293.
- [6] S. C. Zhang, C. J. Rutland, Premixed flame effects on turbulence and pressure-related terms, Combust. Flame 102 (1995) 447–461.
- [7] C. J. Rutland, R. S. Cant, Turbulent transport in premixed flames, Proceedings of the Summer Program, Center for Turbulence Research,
 Stanford University (1994) 75–94.
- [8] A. N. Lipatnikov, J. Chomiak, Effects of premixed flames on turbulence and turbulent scalar transport, Prog. Energy Combust. Sci. 36 (2010)
 1–102.
- [9] O. Desjardins, G. Blanquart, G. Balarac, H. Pitsch, High order conservative finite difference scheme for variable density low Mach number
 turbulent flows, J. Comput. Phys. 227 (2008) 7125–7159.
- 312 [10] J. F. MacArt, M. E. Mueller, Semi-implicit iterative methods for low Mach number turbulent reacting flows: Operator splitting versus approximate factorization, J. Comput. Phys. 326 (2016) 569–595.
- [11] S. G. Davis, A. V. Joshi, H. Wang, F. Egolfopoulos, An optimized kinetic model of H2/CO combustion, Proc. Combust. Inst. 30 (2005)
 1283–1292.
- N. Burali, S. Lapointe, B. Bobbitt, G. Blanquart, Y. Xuan, Assessment of the constant non-unity Lewis number assumption in chemicallyreacting flows, Combust. Theory Model 7830 (2016) 1–26.

- [13] M. M. Rogers, R. D. Moser, Direct simulation of a self-similar turbulent mixing layer, Phys. Fluids 6 (1994) 903–923.
- [14] J. Rotta, Statistische Theorie nichthomogener Turbulenz, Z. Phys. 129 (1951) 547–572.
- [15] J. L. Lumley, Pressure-strain correlation, Phys. Fluids 18 (1975) 750.
- [16] W. P. Jones, Models for turbulent flows with variable density and combustion, in Prediction Methods for Turbulent Flows (W. Kollmann, Ed.), Hemisphere (1980).
- [17] B. Bobbitt, S. Lapointe, G. Blanquart, Vorticity transformation in high Karlovitz number premixed flames, Phys. Fluids 28 (2016) 015101.
- 24 [18] A. Kazbekov, K. Kumashiro, A. M. Steinberg, Enstrophy transport in swirl combustion, J. Fluid Mech. 876 (2019) 715–732.
- 125 [19] C. G. Speziale, Analytical methods for the development of Reynolds-stress closures in turbulence, Annu. Rev. Fluid Mech. 23 (1991) 107–157.
- [20] J. F. MacArt, T. Grenga, M. E. Mueller, Evolution of flame-conditioned velocity statistics in turbulent premixed jet flames at low and high Karlovitz numbers, Proc. Combust. Inst. 37 (2019) 2503–2510.

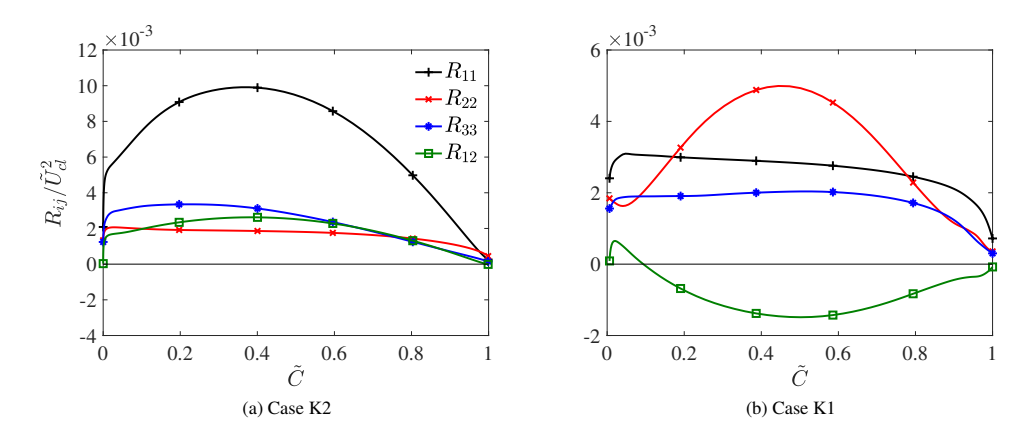


Figure 1: The density-weighted Reynolds stress components, normalized by $\tilde{U}_{\rm cl}^2$, at the streamwise location $x/H_0=3$.

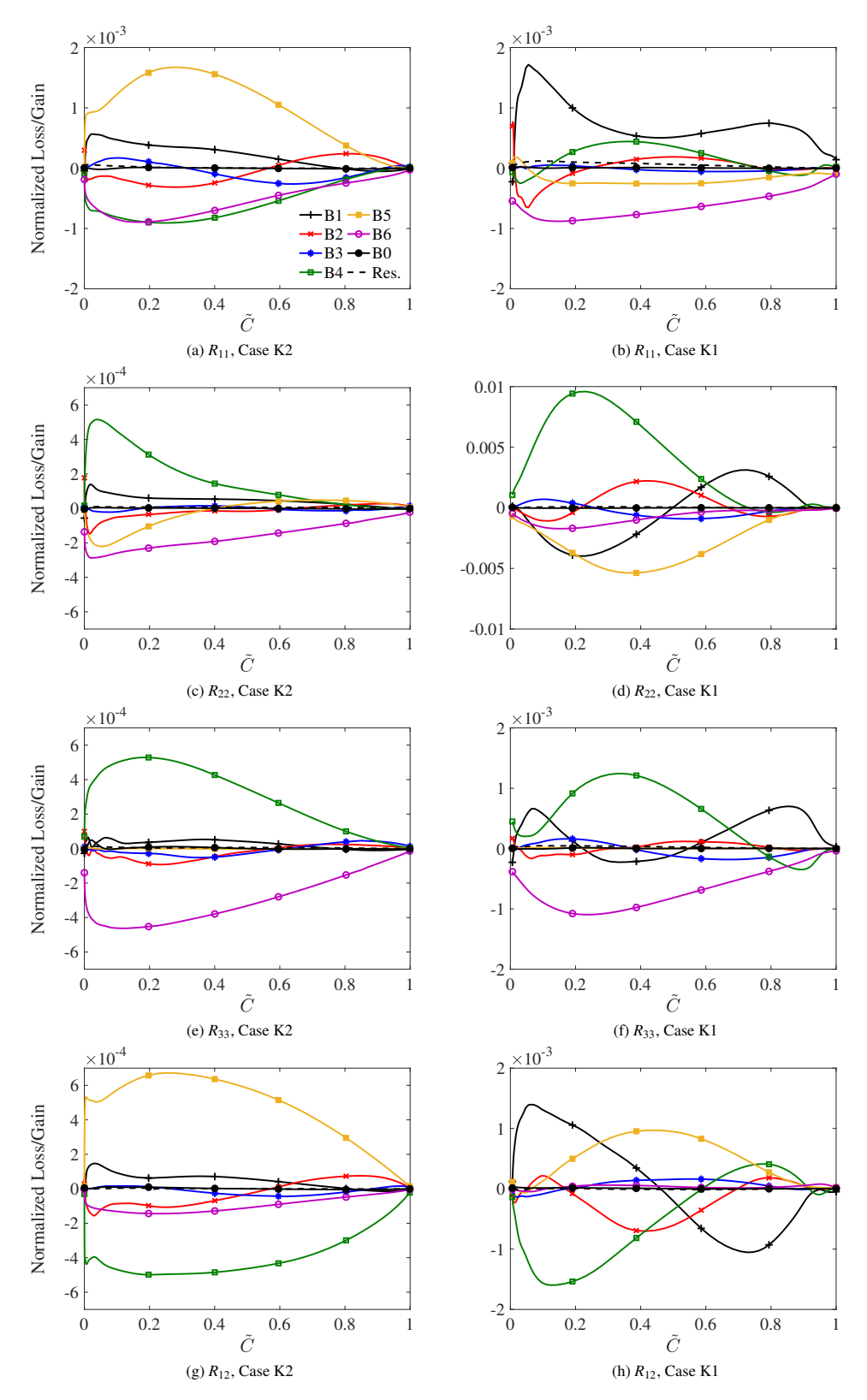


Figure 2: The density-weighted Reynolds stress budgets, normalized by $\bar{\rho}_{cl}\tilde{U}_{cl}^3/y_{1/2}$, at the streamwise location $x/H_0=3$.

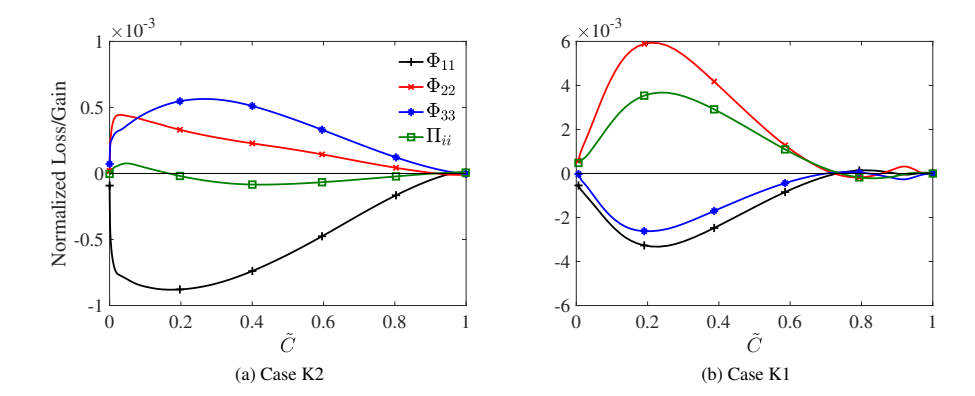


Figure 3: Decomposition of the the velocity-pressure gradient correlation term into the redistribution term and the isotropic term, normalized by $\bar{\rho}_{\rm cl}\tilde{U}_{\rm cl}^3/y_{1/2}$, at the streamwise location $x/H_0=3$.

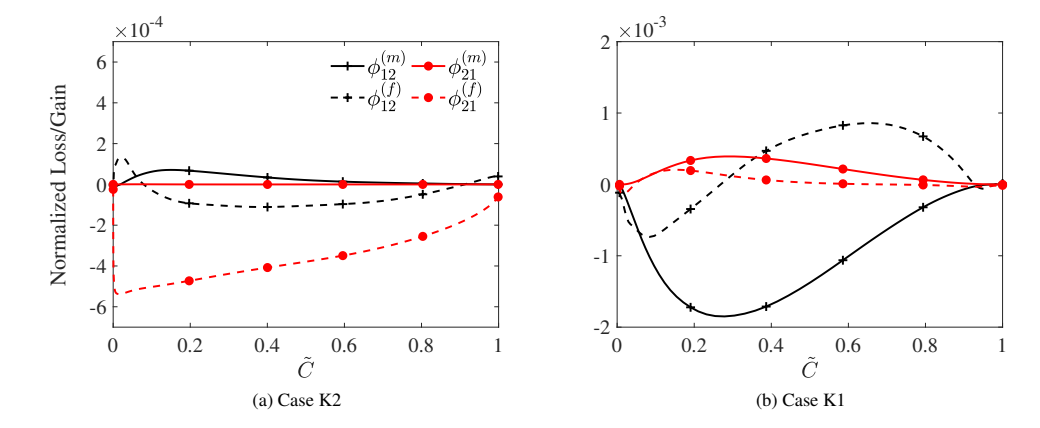


Figure 4: Decomposition of the velocity-pressure gradient correlation term in the budget for R_{12} into the mean pressure term and the fluctuating pressure term, normalized by $\bar{\rho}_{\rm cl}\tilde{U}_{\rm cl}^3/y_{1/2}$, at the streamwise location $x/H_0=3$.

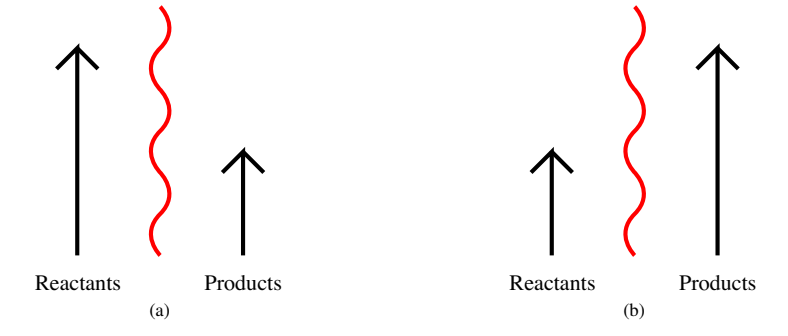


Figure 5: Different configurations of the flame and the reactants/products streams. The flame is indicated by the red wavy lines, and the reactants/products streams are indicated by the black lines with arrows.

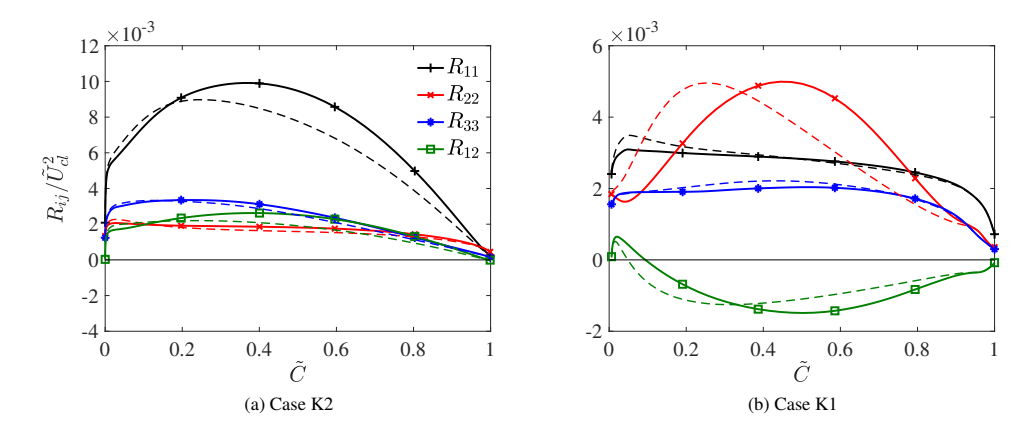


Figure 6: The density-weighted Reynolds stress components (solid lines) with the non-density-weighted Reynolds stress components (dashed lines), where both are normalized by $\tilde{U}_{\rm cl}^2$, at the streamwise location $x/H_0=3$.

Table 1: Relevant DNS parameters [3]

Case	K2	K1
$U_0 (\mathrm{m/s})$	93.4	23.4
H_0 (mm)	1.08	4.32
Re_0	5,000	5,000
Ka _{cr}	6.7	6.7
$Ka_{\tilde{C}=0.5}$	54	3.7
$\mathrm{Da}_{\mathrm{\tilde{C}}=0.5}$	0.05	0.60
Domain $(L \times H \times W)$	$24H_0 \times 16H_0 \times 3H_0$	$12H_0 \times 24H_0 \times 3H_0$
Grid points	$1536 \times 576 \times 256$	$768 \times 586 \times 256$